ECSE 513: Robust Control Systems
Semester: Winter 2020
Final Project Report
Robust H_∞ Controller Design of an Inverted Pendulum

Instructor: Prof. Benoit Boulet
Submitted by: Jilan Samiuddin (ID: 260894931)

April 22, 2020

1 Introduction

The inverted system pendulum is one of the most common systems in control systems textbooks and literature. Figure 1 shows the inverted pendulum on a cart system, where m_c is mass of the cart, m_p is the mass of the pendulum, b is the coefficient of friction for cart, l_p is the length to pendulum center of mass (COM), I is the mass moment of inertia of the pendulum, F_c is the force applied to the cart, x_c is the cart position coordinate, and θ_p is the pendulum angle from vertical (down). Its popularity stems from the fact that without control, the pendulum will always collapse to the ground. In other words, the inverted pendulum system is intrinsically unstable and without a proper controller, it cannot be balanced in the upright position. The balancing is achieved by moving the pivot point horizontally as part of a feedback system, changing the rate of rotation of a mass mounted on the pendulum on an axis parallel to the pivot axis and thereby generating a net torque on the pendulum [1]. A DC motor is generally used to provide the pivotal torque.

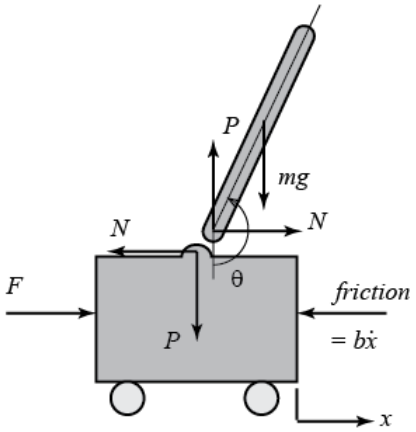

Figure 1: Inverted pendulum on a cart [2]

2 System model

The inverted pendulum on a cart system can be split into two bodies – the DC motor and the inverted pendulum on the cart (IPC) itself. Hence, modeling the DC motor and the IPC separately is common.

2.1 DC Motor

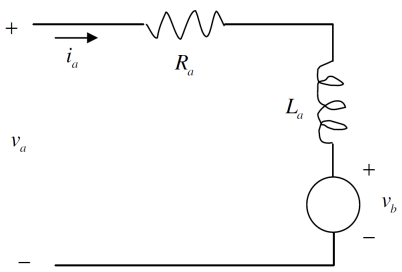

Figure 2: DC Motor schematic [3]

The DC motor, shown in Figure 2, can be modeled using the Kirchoff's voltage law as follows (the electrical equation):

$$v_a = R_a i_a + L_a \frac{di_a}{dt} + v_b \tag{1}$$

where, v_a is the armature voltage, i_a is the armature current, R_a is the armature resistance, L_a is the armature inductance, and $v_b = K_e \omega_m$ is the back emf, where ω_m is the angular velocity of the motor shaft, and K_e is the back emf constant. The mechanical behavior of the motor is described by the following equation:

$$J_m \frac{d\omega_m}{dt} + b_m \omega_m = \tau_m \tag{2}$$

where, J_m is the rotor moment of inertia, b_m is the rotor viscous friction constant, and τ_m is the motor torque. The motor torque is given by

$$\tau_m = K_m i_a \tag{3}$$

where, K_m is the motor torque constant. Combining (1), (2) and (3), the state-space equation for the DC motor is given by

$$\frac{d}{dt}\begin{bmatrix} \omega_m \\ i_a \end{bmatrix} = \begin{bmatrix} -\frac{b_m}{J_m} & \frac{K_m}{J} \\ -\frac{K_e}{L_a} & -\frac{R_a}{L_a} \end{bmatrix} \begin{bmatrix} \omega_m \\ i_a \end{bmatrix} + \begin{bmatrix} 0 \\ \frac{1}{L_a} \end{bmatrix} v_a \tag{4}$$

2.2 Inverted pendulum on the cart

The following model has been derived in [2]. From the free-body diagram shown in Figure 1, the horizontal forces on the cart give the following equation of motion:

$$m_c \ddot{x}_c + b\dot{x}_c + N = F_c, \tag{5}$$

and the horizontal forces on the pendulum give the following equation of motion:

$$N = m_p \ddot{x}_c + m_p l_p \ddot{\theta}_p \cos\theta_p - m_p l_p \dot{\theta}_p^2 \sin\theta_p, \tag{6}$$

where, N is the reaction force. Substituting equation (6) into (5),

$$(m_c + m_p)\,\ddot{x}_c + b\dot{x}_c + m_p l_p \ddot{\theta}_p \cos\theta_p - m_p l_p \dot{\theta}_p^2 \sin\theta_p = F_c. \tag{7}$$

Now, the vertical forces on the pendulum give the following equation of motion:

$$P\sin\theta_p + N\cos\theta_p - m_p g\sin\theta_p = m_p l_p \ddot{\theta}_p + m_p \ddot{x}_c \cos\theta_p \tag{8}$$

Summing the moments about the centroid of the pendulum:

$$-Pl_p\sin\theta_p - Nl_p\cos\theta_p = I\ddot{\theta}_p \tag{9}$$

Combining equations (8) and (9),

$$(I + m_p l_p^2)\ddot{\theta}_p + m_p g l_p \sin\theta_p = -m_p l_p \ddot{x}_c \cos\theta_p \tag{10}$$

Equations (7) and (10) are the governing equations of IPC. To linearize around $x_c = \dot{x}_c = \theta_p = \dot{\theta}_p = 0$, and noting that for small angles $\sin(\theta_p) \cong \theta_p$ and $\cos(\theta_p) \cong 1$, yields the following equations from (7) and (10) respectively:

$$(m_c + m_p)\,\ddot{x}_c + b\dot{x}_c + m_p l_p \ddot{\theta}_p = F_c$$

$$(I + m_p l_p^2)\ddot{\theta}_p + m_p g l_p \theta_p = -m_p l_p \ddot{x}_c$$

from which we have the following state-space model of IPC:

$$\frac{d}{dt}\begin{bmatrix} x_c \\ \dot{x}_c \\ \theta_p \\ \dot{\theta}_p \end{bmatrix} = \begin{bmatrix} 0 & 1 & 0 & 0 \\ 0 & \frac{-(I+m_p l_p^2)b}{I(m_c+m_p)+m_c m_p l_p^2} & \frac{m_p^2 g l_p^2}{I(m_c+m_p)+m_c m_p l_p^2} & 0 \\ 0 & 0 & 0 & 1 \\ 0 & \frac{-m_p l_p b}{I(m_c+m_p)+m_c m_p l_p^2} & \frac{m_p g l_p (m_c+m_p)}{I(m_c+m_p)+m_c m_p l_p^2} & 0 \end{bmatrix} \begin{bmatrix} x_c \\ \dot{x}_c \\ \theta_p \\ \dot{\theta}_p \end{bmatrix} + \begin{bmatrix} 0 \\ \frac{I+m_p l_p^2}{I(m_c+m_p)+m_c m_p l_p^2} \\ 0 \\ \frac{m_p l_p}{I(m_c+m_p)+m_c m_p l_p^2} \end{bmatrix} F_c \tag{11}$$

2.3 Overall model of the system

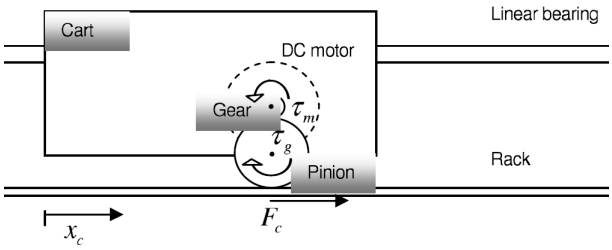

Figure 3: The cart schematic [3]

The cart schematic shown in Figure 3 demonstrates that the torque τ_m produced by the motor is translated into gear torque τ_g which rotates the pinion on the rack. Using the following relations:

$$\omega_g = \frac{1}{k_g}\omega_m, \qquad \tau_m = \frac{1}{k_g}\tau_g, \qquad F_c = \frac{1}{r_g}\tau_g$$

where, r_g is the radius of the pinion, ω_g is the angular velocity of the gear, τ_g is the gear torque, and k_g is the gear ratio, we have

$$F_c = \frac{1}{r_g}\tau_g = \frac{\tau_m k_g}{r_g} \overset{(3)}{=} \left(\frac{K_m k_g}{r_g}\right) i_a \tag{12}$$

Equation (12) can be further break-down as follows:

$$\begin{aligned} F_c &= \frac{K_m k_g}{r_g}\left(\frac{v_a - v_b}{R_a}\right) = \frac{K_m k_g}{r_g}\left(\frac{v_a - K_e\omega_m}{R_a}\right) \\ &= \frac{K_m k_g}{r_g}\left(\frac{v_a - K_e\omega_g k_g}{R_a}\right) = \frac{K_m k_g}{r_g R_a}\left(v_a - K_e k_g \frac{d\theta_g}{dt}\right) \\ &= \frac{K_m k_g}{r_g R_a}\left(v_a - \frac{K_e k_g}{r_g}\frac{dx_g}{dt}\right) = \frac{K_m k_g}{r_g R_a}\left(v_a - \frac{K_e k_g}{r_g}\frac{dx_c}{dt}\right) \\ \Rightarrow F_c &= \alpha v_a - \beta \dot{x}_c \end{aligned} \tag{13}$$

here, $\alpha = \frac{k_g K_m}{r_g R_a}$ and $\beta = \frac{k_g^2 K_m K_e}{r_g^2 R_a}$. So, substituting equation (13) into (11), the overall system can be represented using the following state-space equation:

$$\begin{aligned} \frac{d}{dt}\begin{bmatrix} x_c \\ \dot{x}_c \\ \theta_p \\ \dot{\theta}_p \end{bmatrix} &= \begin{bmatrix} 0 & 1 & 0 & 0 \\ 0 & \frac{-(I+m_p l_p^2)b}{I(m_c+m_p)+m_c m_p l_p^2} & \frac{m_p^2 g l_p^2}{I(m_c+m_p)+m_c m_p l_p^2} & 0 \\ 0 & 0 & 0 & 1 \\ 0 & \frac{-m_p l_p b}{I(m_c+m_p)+m_c m_p l_p^2} & \frac{m_p g l_p (m_c+m_p)}{I(m_c+m_p)+m_c m_p l_p^2} & 0 \end{bmatrix}\begin{bmatrix} x_c \\ \dot{x}_c \\ \theta_p \\ \dot{\theta}_p \end{bmatrix} \cdots \\ &\quad \cdots + \begin{bmatrix} 0 \\ \frac{I+m_p l_p^2}{I(m_c+m_p)+m_c m_p l_p^2} \\ 0 \\ \frac{m_p l_p}{I(m_c+m_p)+m_c m_p l_p^2} \end{bmatrix}(\alpha v_a - \beta \dot{x}_c) \\ &= \begin{bmatrix} 0 & 1 & 0 & 0 \\ 0 & \frac{-(I+m_p l_p^2)b}{I(m_c+m_p)+m_c m_p l_p^2} & \frac{m_p^2 g l_p^2}{I(m_c+m_p)+m_c m_p l_p^2} & 0 \\ 0 & 0 & 0 & 1 \\ 0 & \frac{-m_p l_p b}{I(m_c+m_p)+m_c m_p l_p^2} & \frac{m_p g l_p (m_c+m_p)}{I(m_c+m_p)+m_c m_p l_p^2} & 0 \end{bmatrix}\begin{bmatrix} x_c \\ \dot{x}_c \\ \theta_p \\ \dot{\theta}_p \end{bmatrix} \cdots \\ &\quad \cdots + \begin{bmatrix} 0 \\ \frac{\alpha(I+m_p l_p^2)}{I(m_c+m_p)+m_c m_p l_p^2} \\ 0 \\ \frac{\alpha m_p l_p}{I(m_c+m_p)+m_c m_p l_p^2} \end{bmatrix} v_a + \begin{bmatrix} 0 \\ \frac{-\beta(I+m_p l_p^2)}{I(m_c+m_p)+m_c m_p l_p^2} \\ 0 \\ \frac{-\beta m_p l_p}{I(m_c+m_p)+m_c m_p l_p^2} \end{bmatrix}\dot{x}_c \\ \Rightarrow \frac{d}{dt}\begin{bmatrix} x_c \\ \dot{x}_c \\ \theta_p \\ \dot{\theta}_p \end{bmatrix} &= \begin{bmatrix} 0 & 1 & 0 & 0 \\ 0 & \frac{-(I+m_p l_p^2)b}{I(m_c+m_p)+m_c m_p l_p^2} - \frac{\beta(I+m_p l_p^2)}{I(m_c+m_p)+m_c m_p l_p^2} & \frac{m_p^2 g l_p^2}{I(m_c+m_p)+m_c m_p l_p^2} & 0 \\ 0 & 0 & 0 & 1 \\ 0 & \frac{-m_p l_p b}{I(m_c+m_p)+m_c m_p l_p^2} - \frac{\beta m_p l_p}{I(m_c+m_p)+m_c m_p l_p^2} & \frac{m_p g l_p (m_c+m_p)}{I(m_c+m_p)+m_c m_p l_p^2} & 0 \end{bmatrix}\begin{bmatrix} x_c \\ \dot{x}_c \\ \theta_p \\ \dot{\theta}_p \end{bmatrix} \cdots \\ &\quad \cdots + \begin{bmatrix} 0 \\ \frac{\alpha}{m_c} \\ 0 \\ -\frac{\alpha}{m_c l_p} \end{bmatrix} v_a \end{aligned} \tag{14}$$

2.4 System Parameters

The values of the system parameters are given in Table 1.

Parameter	Description	Nominal Value
K_m	Torque proportionality constant	0.0077 Nm/A
K_e	Back electromotive proportionality constant	0.0077 V/rad/s
R_a	Armature resistance	2.6 Ω
J_m	Rotor moment of inertia	2×10^{-5} kg m^2
b_m	Rotor viscous friction constant	10^{-6} kg m^2/s
L_a	Armature inductance	180 μH
m_c	Mass of the cart	0.326 kg
m_p	Mass of the pendulum	0.106 kg
l_p	Length to pendulum center of mass	0.168 m
b	Coefficient of friction of the cart	10^{-3} N/m/sec
I	Mass moment of inertia of the pendulum	0.006 kg m^2
g	Gravitational acceleration	9.8 m$^2/s$
k_g	Internal Gear Ratio	3.7
r_g	Motor Gear Radius	0.0064 m
v_a	Limit: ±5 V	N/A

Table 1: System parameters [4]

3 Control Design, Analysis and Performance

Although it is very common to design a controller for the system equation (14), it also should be realized that the actuator, i.e. the DC motor, is a system on its own and may not give the exact control input to the IPC required to balance the pendulum in the upright position. This is mainly because of the uncertainties present in the parameters of the DC motor itself. In this section, a separate controller for the actuator is proposed along with the controller for the IPC as shown in Figure 4.

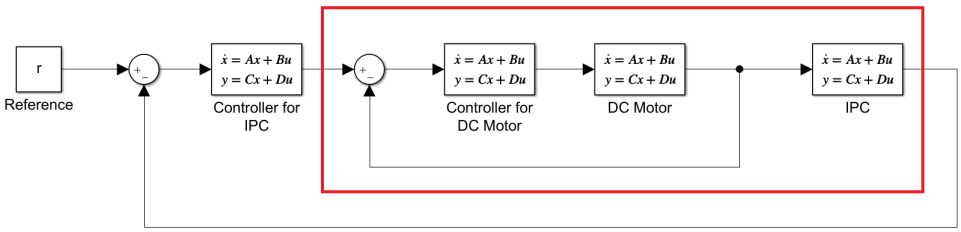

Figure 4: Block diagram showing separate controllers

3.1 Control design for DC motor

As mentioned earlier, the parameters R_a, L_a, K_e, J ,b_m and K_m, of the DC motor have uncertainties. To ensure robust performance of the DC motor in the presence of

uncertainties, a robust H-infinity controller is designed using the additive uncertainty model as shown in Figure 5. The augmented system P is given by

$$P = \begin{bmatrix} 0 & W_a(s) \\ W_e(s) & -G(s)W_e(s) \\ 1 & -G(s) \end{bmatrix}$$

where, $W_a(s) = \frac{1.44s+0.06}{1.15s+1}$ and $W_e(s) = \frac{500}{10s+1}$ are chosen and $G(s)$, the DC motor plant, is obtained using equations (4) and (12), i.e., v_a is the input and F_c is the output of $G(s)$. Using the MATLAB robust control toolbox (see Appendix A for code), the following 5^{th}-order controller for DC motor is obtained:

$$K_{mot}(s) = \frac{60.528(s + 1.444 \times 10^4)(s + 1.19)(s + 0.8697)(s + 0.1)}{(s + 1.455 \times 10^4)(s + 0.1001)(s + 0.09989)(s^2 + 0.1692s + 0.03571)} \tag{15}$$

To achieve the above controller, we obtained $\gamma = 0.9844$.

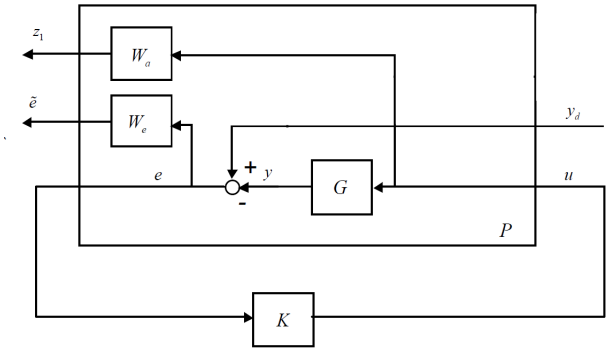

Figure 5: Block diagram for additive uncertainty

3.1.1 Analysis of robustness and performance

The magnitude of the frequency response of the weighting function $W_a(s)$ showing how it covers various admissible perturbations of the DC motor is demonstrated in Figure 6.

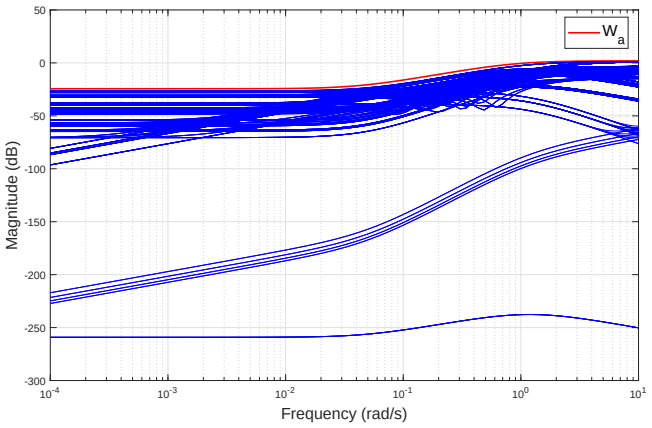

Figure 6: $W_a(s)$ enveloping all the possible perturbed models for the additive uncertainty

The frequency response of the output sensitivity $S = (1 + GK)^{-1}$ of the design together with the weighting functions are given in Figure 7 and Figure 8. Robust stability was achieved since $|K(j\omega)S(j\omega)| < |W_a^{-1}(j\omega)|$ for all frequencies, and also nominal performance was achieved since $|S(j\omega)| < |W_e^{-1}(j\omega)|$ for all frequencies.

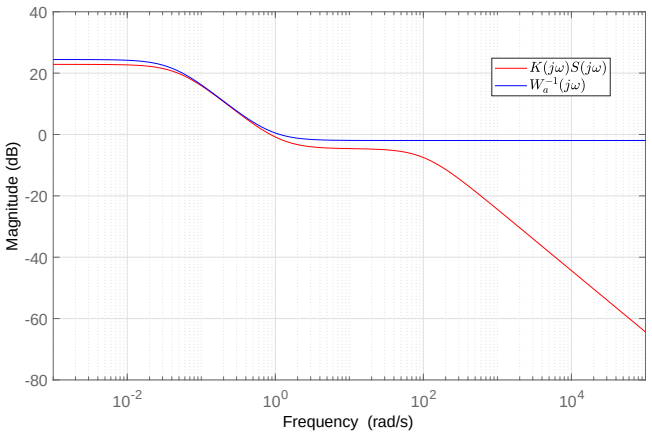

Figure 7: Frequency response of $K(j\omega)S(j\omega)$ versus $W_a^{-1}(j\omega)$

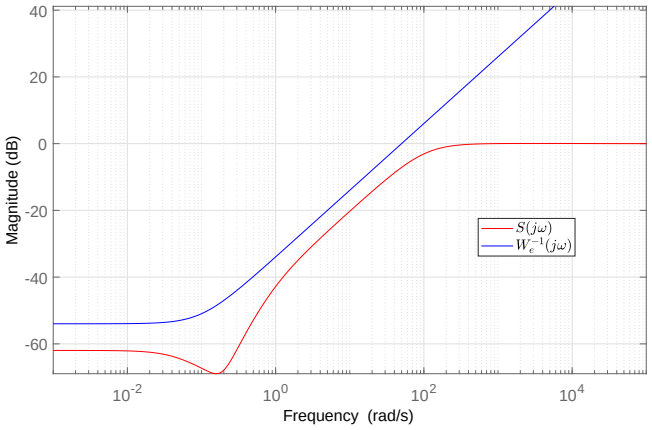

Figure 8: Frequency response of $S(j\omega)$ versus $W_e^{-1}(j\omega)$

3.1.2 Controller performance

The controller's performance on various perturbed models of the DC motor was tested. It was assumed that all the six parameters of the DC motor, R_a, L_a, K_e, J ,b_m and K_m, are uncertain to within ± 50. The performance of the controller is shown in Figure 9. The initial reference was set at 1N, but then was changed to 5N at $t = 5$s. It can be seen that, for various perturbed models, the controller is performing extremely well; the responses for various perturbed model have almost overlapped each other despite step changes in the reference value.

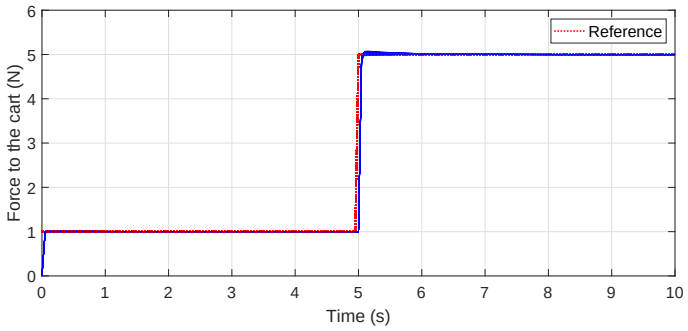

Figure 9: Step response for the DC motor with controller

3.2 Control design for IPC

For the configuration shown in Figure 10, where G represents IPC (without cascading the DC motor) and K the controller to be designed, weighting functions W_1, W_2 and W_3 can be appended as shown in Figure 11 [5]. The following weights are defined:

$$W_1 = \frac{0.1s + 0.6675}{s + 0.445}, \qquad W_2 = 0.0001, \qquad W_3 = \frac{10s + 1000}{s + 10000},$$

where, task of W_1 is to ensure good reference-tracking and disturbance-rejection performance, task of W_2 is to limit control effort, task of W_3 is to ensure robustness and noise attenuation. Using mixed-sensitivity loop shaping [5], the following H_∞ controller is obtained:

$$K = \begin{bmatrix} \frac{-2589.4(s+19.52)(s+8.781)(s+10000)^2(s+0.00231)(s+0.0001682)}{(s-15.5)(s+1.526)(s+0.445)(s+9998)(s+10000)(s^2+336.2s+3.949\times10^4)} \\ \\ \frac{77287(s+10000)^2(s+8.781)(s+0.05712)(s+0.002312)(s+0.0001196)}{(s-15.5)(s+1.526)(s+0.445)(s+9998)(s+10000)(s^2+336.2s+3.949\times10^4)} \end{bmatrix}^T \tag{16}$$

with $\gamma = 1.5032$. The controller design was focused on robustness to disturbance and measurement noise rather than uncertainties in the model with the assumption that there are no uncertainties in the physical parameters of IPC.

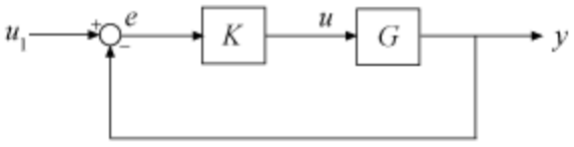

Figure 10: Feedback interconnection of plant with controller [5]

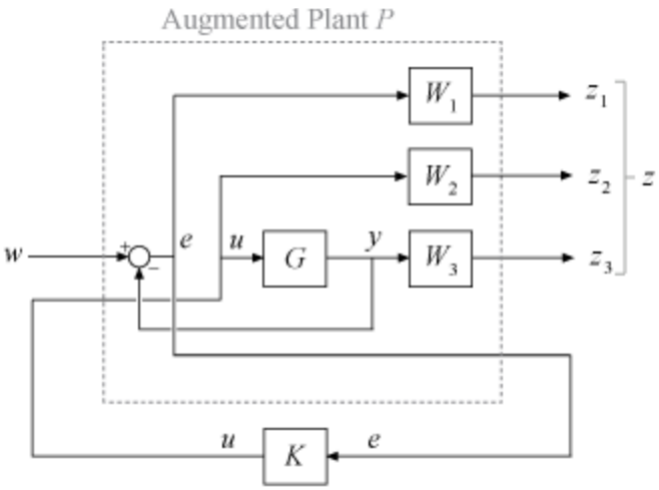

Figure 11: Weights appended to standard feedback interconnection [5]

3.2.1 Analysis of robustness and performance

From Figure 12, it can be seen that $|S(j\omega)| < \left|W_1^{-1}(j\omega)\right|$ for all frequencies except for the pair $\theta \to e_\theta$, and thus nominal performance was not achieved. However, robust stability and noise attenuation was ensured as suggested by Figure 13, since for all frequencies it can be seen that $|T(j\omega)| < \left|W_3^{-1}(j\omega)\right|$.

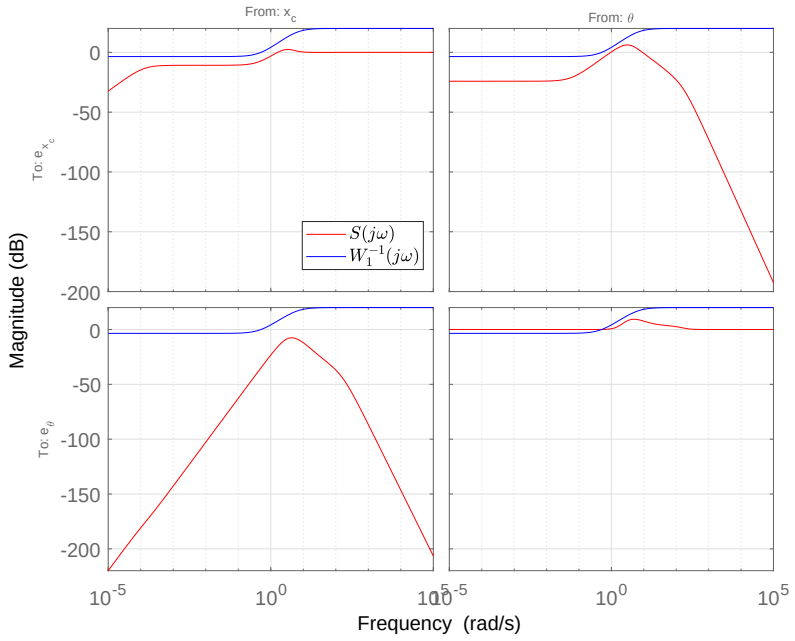

Figure 12: Frequency response of $S(j\omega)$ versus $W_1^{-1}(j\omega)$

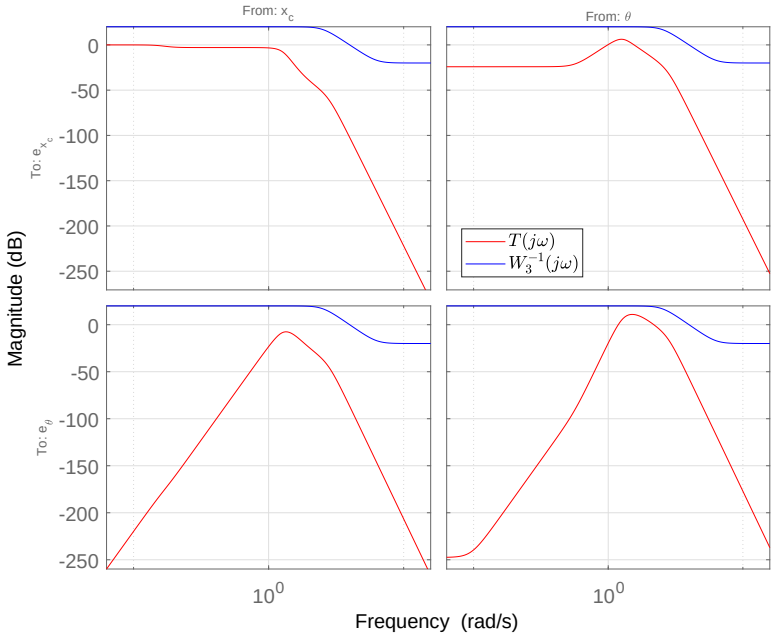

Figure 13: Frequency response of $T(j\omega)$ versus $W_3^{-1}(j\omega)$

3.2.2 Controllers' performances

Using the configuration shown in Figure 4, the controller (16) (labeled as "*Controller for IPC*") is integrated with the controller (15) (labeled as "*Controller for* DC Motor") to complete the overall feedback system.

At first, impulse disturbances through the θ_p channel was introduced to the system to test the controller's performance. An impulse of 0.1 radian and -0.1 radian at (approximately) 2 second and 7 second respectively was introduced. It can be seen from Figure 14 that it took approximately 2 seconds to reject the disturbances in both the instances before tracking the reference signal once again. The DC motor controller (15) was also able to meet the demand of the IPC controller (16) as can be seen from Figure 15. Also, the controller did not violate the constraints on the magnitude of the supply voltage.

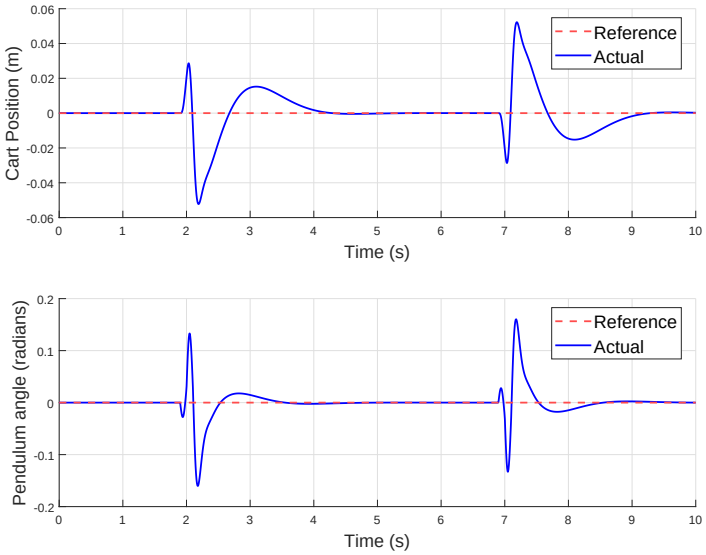

Figure 14: Output response to impulse disturbances

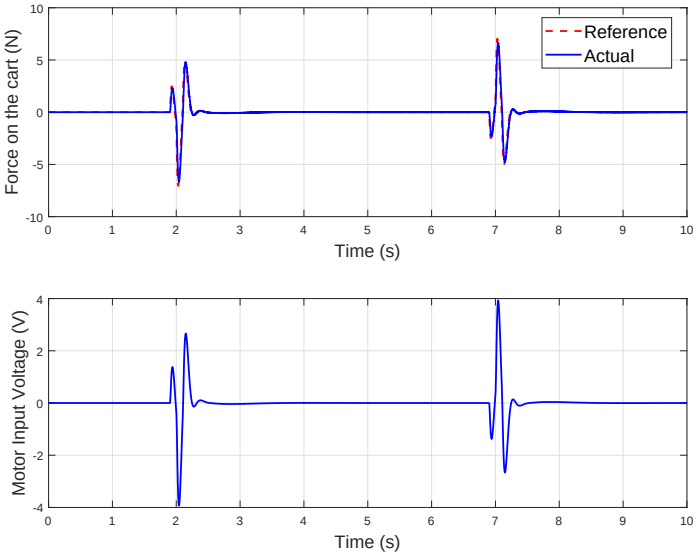

Figure 15: Output response to impulse disturbances

Next, the disturbance was removed from the system and measurement noise was added only. It can be seen from Figure 16 that the controller was able to attenuate the effect of the measurement noise while maintaining the tracking performance at a satisfactory level. The DC motor controller (15) was also able to meet the demand of the IPC controller (16) as can be seen from Figure 15. Also, the controller did not violate the constraints on the magnitude of the supply voltage.

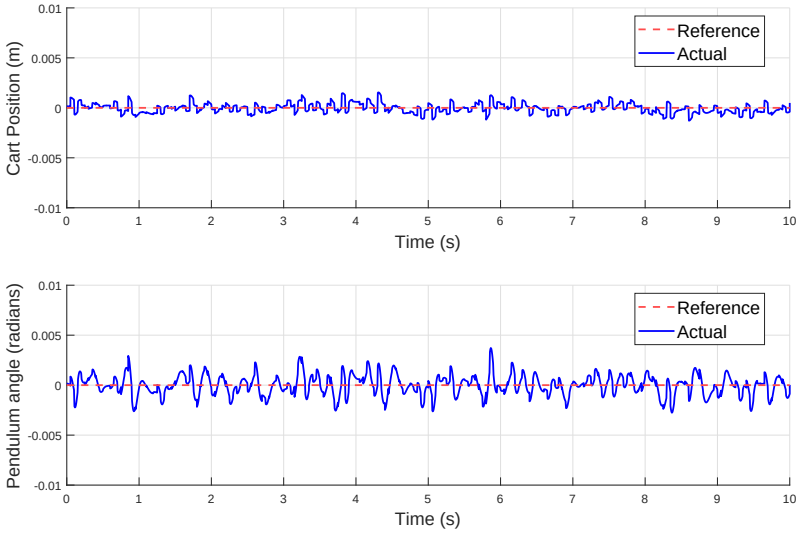

Figure 16: Output response to measurement noise

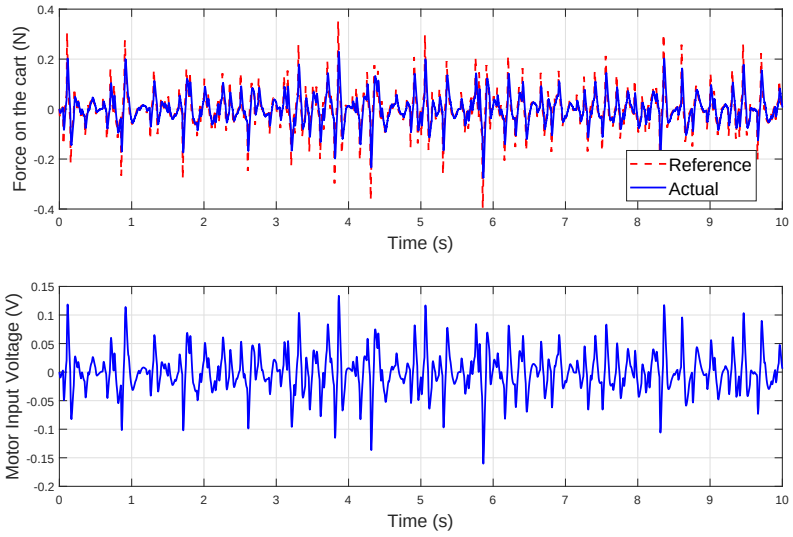

Figure 17: Input response to measurement noise

Finally, both impulse disturbances and measurement noise was added to the system. It can be seen from Figure 18 that again it took approximately 2 seconds to reject the disturbances in both the instances before tracking the reference signal once again while attenuating measurement noise as well. The DC motor controller (15) was also able to meet the demand of the IPC controller (16) as can be seen from Figure 19. Also, the controller did not violate the constraints on the magnitude of the supply voltage.

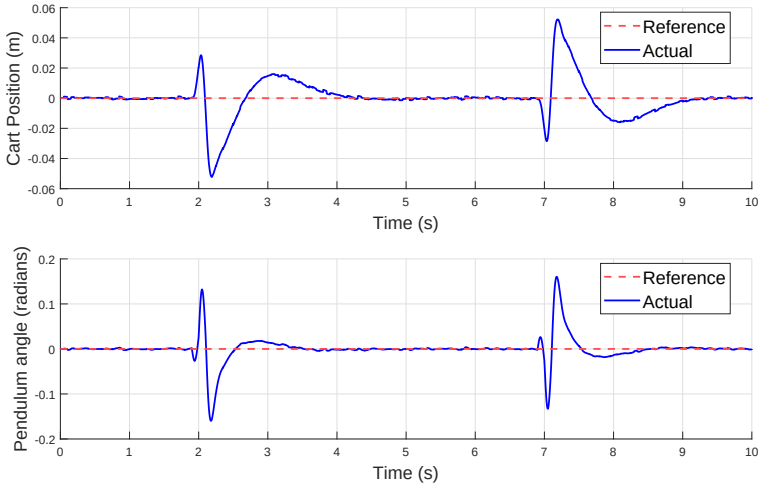

Figure 18: Output response to impulse disturbance and measurement noise

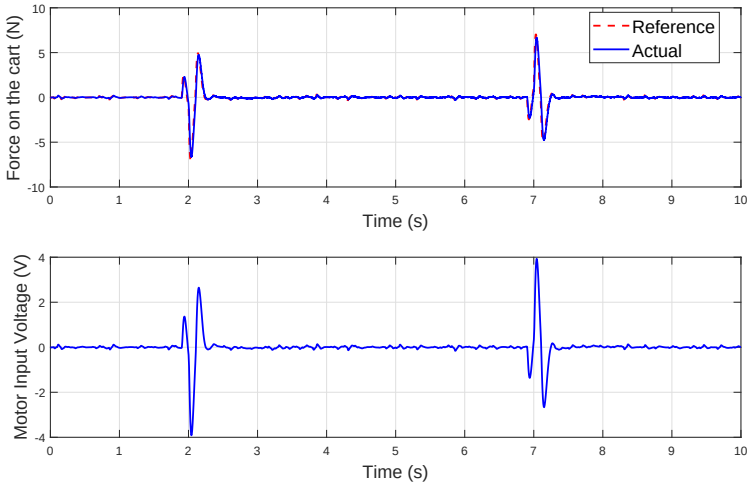

Figure 19: Input response to impulse disturbance and measurement noise

3.3 Control design for IPC cascaded with DC motor (and its controller)

In this section, a controller is obtained for the IPC cascaded with the DC motor (and its controller), i.e, G in Figure 10 represents the system within the red box in Figure 4. The purpose of this section is to compare the performance of the controller designed in this setup compared to controller designed in the setup described in Section 3.2.
Using mixed-sensitivity loop shaping [5], the following H_∞ controller is obtained:

$$K = \begin{bmatrix} \frac{-6353s^7 - 8.018\times10^5 s^6 - 1.608\times10^7 s^5 - 9.192\times10^7 s^4 - 7.277\times10^7 s^3 - 3.577\times10^6 s^2 - 8277s - 0.9031}{s^8 + 298.2s^7 + 3.906\times10^4 s^6 + 2.166\times10^6 s^5 - 7.854\times10^7 s^4 - 2.98\times10^8 s^3 - 3.555\times10^8 s^2 - 1.439\times10^8 s - 6.345\times10^6} \\ \\ \frac{7.789\times10^4 s^7 + 8.787\times10^6 s^6 + 7.96\times10^7 s^5 + 7.548\times10^7 s^4 + 1.137\times10^7 s^3 + 4.081\times10^5 s^2 + 908.2s + 0.0545}{s^8 + 298.2s^7 + 3.906\times10^4 s^6 + 2.166\times10^6 s^5 - 7.854\times10^7 s^4 - 2.98\times10^8 s^3 - 3.555\times10^8 s^2 - 1.439\times10^8 s - 6.345\times10^6} \end{bmatrix}^T \tag{17}$$

Only the impulse disturbance test is carried out to compare the performances. Same as before, an impulse of 0.1 radian and -0.1 radian at (approximately) 2 second and 7 second respectively was introduced. It can be seen from Figure 20 that it took approximately 2 seconds to reject the disturbances in both the instances before tracking the reference signal once again. Although the disturbances were successfully rejected, both the cart position and the pendulum angle peaked higher in magnitude compared to Figure 14 during the disturbances. The DC motor controller (15) was also able to meet the demand of the controller (17) as can be seen from Figure 21. However, the controller did violate the constraints on the magnitude of the supply voltage exceeding the magnitude of 5V (the constraint value) when trying to reject the disturbances.

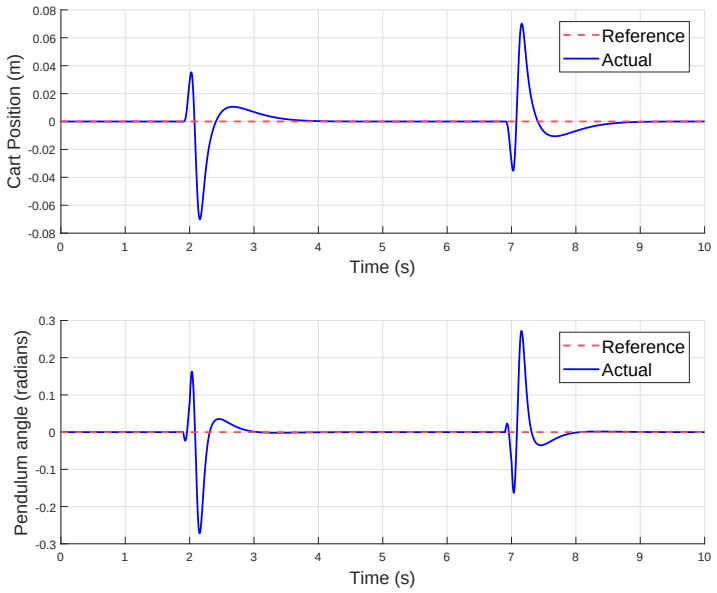

Figure 20: Output response to impulse disturbances

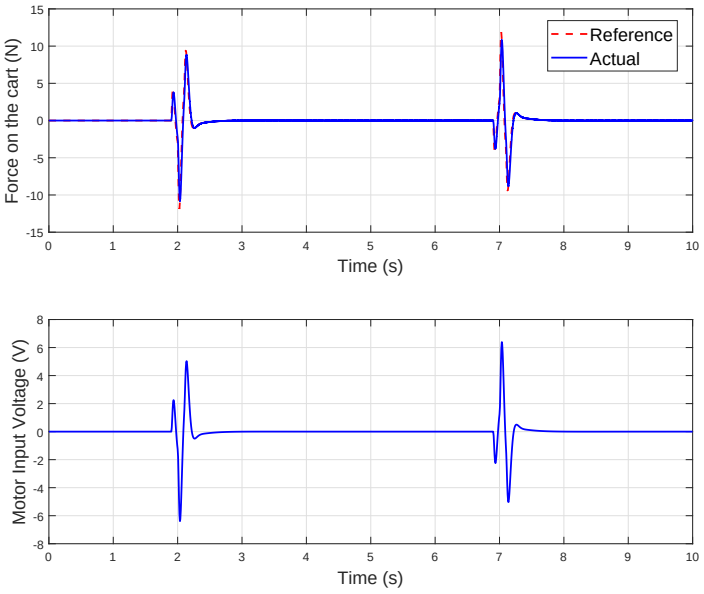

Figure 21: Output response to impulse disturbances

4 Conclusion

The purpose of this project was to design a robust H_∞ controller for the IPC. In order to do so, the system was split into two parts – the actuator, i.e., the DC motor, and the IPC itself. At first, an H_∞ controller was designed for the DC motor to ensure robustness to parameter uncertainties when responding to the requirement by the IPC. In the process, nominal performance of the controller was also guaranteed. Next, an H_∞ controller was designed for the IPC using mixed-sensitivity with the assumption that there are no uncertainties in the parameters of the mechanical part of the system. This allowed to concentrate on measurement noise attenuation and disturbance rejection while designing the controller. Nominal performance, robust stability and noise attenuation for the IPC was ensured through the designed controller. The controllers were tested under different conditions and overall, the performance was very satisfactory.

References

[1] Inverted pendulum. https://en.wikipedia.org/wiki/Inverted_pendulum. Last Accessed: 2020-04-12.

[2] Inverted pendulum: System modeling. http://ctms.engin.umich.edu/CTMS/index.php?example=InvertedPendulum&section=SystemModeling. Last Accessed: 2020-04-12.

[3] Lecture 2: Dc motor and cart, ecse 493 control and robotics laboratory, department of electrical and computer engineering, mcgill university, 2016.

[4] Control and robotics laboratory: Ecse 493 lab manual, department of electrical and computer engineering, mcgill university, 2016.

[5] Mixed-sensitivity loop shaping. https://www.mathworks.com/help/robust/gs/using-mixsyn-for-h-infinity-loop-shaping.html. Last Accessed: 2020-04-12.